


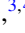



## Kuramoto synchronization of quantum tunneling polarons for describing the dynamic structure in cuprate superconductors

Victor Velasco <sup>1,\*</sup> Marcello B. Silva Neto <sup>1</sup> Andrea Perali <sup>2</sup> Sandro Wimberger <sup>3,4</sup>  
Alan R. Bishop<sup>5</sup> and Steven D. Conradson <sup>6,7</sup>

<sup>1</sup>*Instituto de Física, Universidade Federal do Rio de Janeiro, Caixa Postal 68528, Rio de Janeiro, Brazil*

<sup>2</sup>*School of Pharmacy, Physics Unit, Università di Camerino, Via Madonna delle Carceri 9, 62032 Camerino, Italy*


<sup>3</sup>*Dipartimento di Scienze Matematiche, Fisiche, e Informatiche, Università di Parma, 43124 Parma, Italy*

<sup>4</sup>*INFN, Sezione di Milano Bicocca, Gruppo Collegato di Parma, 43124 Parma, Italy*

<sup>5</sup>*Center for Nonlinear Studies, Los Alamos National Laboratory, Los Alamos, New Mexico 87545, USA*

<sup>6</sup>*Department of Complex Matter, Josef Stefan Institute, 1000 Ljubljana, Slovenia*

<sup>7</sup>*Department of Chemistry, Washington State University, Pullman, Washington 99164, USA*

 (Received 17 September 2021; revised 5 May 2022; accepted 5 May 2022; published 20 May 2022)

A major open topic in cuprates is the interplay between the lattice and electronic dynamics and the importance of their coupling to the mechanism of high-temperature superconductivity (HTSC). As evidenced by extended x-ray absorption fine structure (EXAFS) experiments, anharmonic structural effects are correlated with the charge dynamics and the transition to a superconducting phase in different HTSC compounds. Here we describe how structural anharmonic effects can be coupled to electronic and lattice dynamics in cuprate systems by performing the exact diagonalization of a prototype anharmonic many-body Hamiltonian on a relevant 6-atom cluster and show that the EXAFS results can be understood as a Kuramoto synchronization transition between coupled internal quantum tunneling of polarons associated with the two-site distribution of the copper–apical oxygen (Cu-O<sub>ap</sub>) pair in the dynamic structure. The transition is driven by the anharmonicity of the lattice vibrations and promotes the pumping of charge, initially stored at the apical oxygen reservoirs, into the copper-oxide plane. Simultaneously, a finite projection of the internal quantum tunneling polaron extends to the copper–planar oxygen (Cu-O<sub>pl</sub>) pair. All these findings allow an interpretation based on an effective quantum-mechanical triple-well potential associated with the oxygen sites of the 6-atom cluster, which accurately represents the phase synchronization of apical oxygens and lattice-assisted charge transfer to the CuO<sub>2</sub> plane.

DOI: [10.1103/PhysRevB.105.174305](https://doi.org/10.1103/PhysRevB.105.174305)

### I. INTRODUCTION

A noted characteristic of cuprates is anomalies in their phonon spectra in a range below 100 meV. Often with distinct, unusual O-isotope dependence, these have been observed in infrared (IR) [1–3], Raman [4], neutron scattering [5], photoemission [6–9], and resonant inelastic x-ray spectroscopies [10–12]. In such a complex, disordered material, the descriptions of the electron-lattice coupling provided by the unusual behaviors of the peak energies and shapes are insufficient to assist in the development of microscopic models of the superconductivity and other properties of interest. Insofar as the vibrations of the atoms that produce the spectra are defined by the potentials between the atoms, a more direct measure of these anharmonic potentials is found in a real space conjugate to the phonon spectra, namely a snapshot of the atom positions over a large volume of the lattice revealed in the pair distributions. Since these distributions are determined by the underlying pair potentials, not only the presence but also the type and extent of anharmonicity are visualized in the pair distribution functions of the dynamic structure factor,  $S(Q, E)$ . This quantity is easily intuited in liquids, where the

positions of atoms in rapid transit between quasistable relative locations are identified in the van Hove function derived from inelastic scattering data [13]. It also occurs in solids in the analogous movements of atoms between locations of similar energies, subject to the constraint that their paths must avoid collisions with the other atoms at their more fixed locations in the solid.

One of the many unusual characteristics of cuprates is the two-site copper-oxygen distributions that are constituents of their dynamic structure. Inelastic neutron scattering measurements identified these shortly after the initial discovery of high-temperature superconductivity [14,15]. However, extended x-ray absorption fine structure (EXAFS) spectroscopy has been the predominant source of these observations because of the relative ease of its measurement of the instantaneous structure factor,  $S(q, t = 0)$  [16,17], with a precision that matches the deviations of  $S(Q, E)$  from the static structure factor,  $S(Q, E = 0)$ . These two-site distributions indicative of anharmonic, double-well potentials were initially observed in the apical Cu-O<sub>ap</sub> pairs [18–24], then in the planar oxygen (O<sub>pl</sub>) of the CuO<sub>2</sub> planes in other cuprates [25–32]. This has been followed by reports of similar behavior in superconducting bismuthates [33,34] and even pnictides [35]. Their observed fluctuations at and through the transitions demonstrated their coupling and even their contribution [36]

\*Corresponding author: [velasco@if.ufrj.br](mailto:velasco@if.ufrj.br)

to the superconductivity. More recently, experiments on overdoped superconducting cuprates have revealed the coupling of the highly disordered Cu-Sr pair, and massive changes in the dynamic structure of Cu-O pairs at the superconducting transition of  $\text{Sr}_2\text{CuO}_{3.3}$  [37]. It is likely that this critical aspect of two-site distributions is a unifying element of high-temperature superconductivity and an indication of strong, nonadiabatic, complex electron-phonon/lattice coupling.

We describe below how the two-site distributions can originate as features of small polarons caused by the doping and mixed-valence character of the materials. Small polarons are defined as a charge inhomogeneity around a central atom and the accompanying local lattice distortion as the neighboring atoms shift their positions to accommodate the different charge. One of their central features is their thermally activated or quantum center of mass tunneling through the lattice. The two-site distribution would occur as a subset of small polarons when the highest occupied states of the system have significant oxygen  $2p$  density. In this case, instead of the hole being confined to the central metal, a fraction of it will reside on one of its neighboring oxygen atoms. This would be expected to result in a second oxygen position at a somewhat longer distance, giving the two-site distribution without perturbing the crystal structure. In the typical transition metal oxide where the metal has equivalent oxygen nearest neighbors, these oxygen ions could exchange the charge and bond length among themselves by temperature-independent quantum tunneling. While this process does shift the site where they reside, in contrast to the small polaron that roams through the lattice, the locations of these modified oxygen atoms are constrained to the nearest-neighbor shell of the metal associated with the excess charge. The crucial point is that this process occurs within the parent polaron, constituting internal dynamics in contrast to the lattice dynamics of the parent. When this tunneling frequency is *high* compared to the hopping frequency of the parent polaron, what we term an internal quantum tunneling polaron (IQTP) is obtained.

In our earlier work on this IQTP problem we used exact diagonalization calculations for a minimal, three-atom, O-Cu-O cluster with an excess hole [Fig. 1(b)] [16,21–23,38] to confirm the experimental signature of IQTPs via the difference between the crystallographic, static structure and probes of the dynamic structure that exhibit the two-site distributions. These results validated both the experimental results and the application of such calculations for incorporating local quantum tunneling dynamics. We noted that dynamical contributions were also added in calculations of fluctuating stripes in the  $\text{CuO}_2$  planes [39] and in charge flux among the apical cation, apical anion, and the in-plane  $\text{CuO}_4$  unit [40].

However, these reports do not address the full anharmonicity and its connection with the double-well potential in the IQTPs. We do so here via two expansions of the original three-atom calculations. Since the most common moiety is not the linear, O-Cu-O cluster found only in single-layer cuprates, but is a Cu surrounded by the  $\text{O}_{\text{pl}}$  atoms with a single  $\text{O}_{\text{ap}}$  [Fig. 1(a)], we incorporate the requisite two  $\text{O}_{\text{ap}}$  atoms by including two, neighboring Cu- $\text{O}_{\text{ap}}$  pairs. Adding the  $\text{O}_{\text{pl}}$  atom that bridges them incorporates the

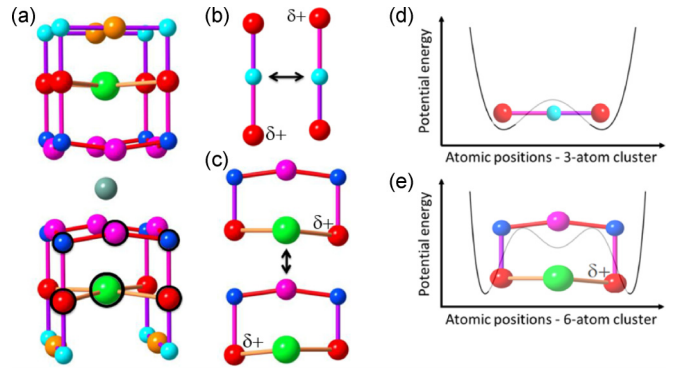


FIG. 1. Relevant structures. (a) The  $\text{YBa}_2\text{Cu}_3\text{O}_7/\text{YSr}_2\text{Cu}_3\text{O}_7$  crystal structure shows the features of multilayered cuprates with higher  $T_c$ 's: two conducting  $\text{CuO}_2$  planes [blue Cu(2) and magenta  $\text{O}_{\text{pl}}$  atoms] bridged by the intervening Y (gray), the charge reservoir consisting in this class of materials of Cu-O chains [turquoise Cu(1) and orange O], and the dielectric layer composed of the  $\text{O}_{\text{ap}}$  (red) and Sr (green). (b) The original three-atom IQTP derived from the two-site Cu(1)- $\text{O}_{\text{ap}}$  distribution found in  $\text{YBa}_2\text{Cu}_3\text{O}_7$  showing its oscillations between its two configurations denoted by the location of the extra hole ( $+\delta$ ) and expanded Cu-O distance [17]. (c) The atoms circled in black in (a) form the six-atom cluster used here. Its excess charge and displacement tunnel between the two Cu(2)- $\text{O}_{\text{ap}}$  pairs through the  $\text{O}_{\text{pl}}$  charge transfer bridge. (d) For the three-atom cluster the potential energy corresponds to a double-well structure [21]. (e) For the 6-atom cluster, the potential energy corresponds to a triple-well structure.

$\text{CuO}_2$  planes. Finally, attending to the finding of the anharmonicity of the  $\text{Sr}^{2+}$  alkaline earth dication [41] and its coupling to the superconductivity [37,42], we include this link to the apical oxygen sites that completes the dielectric layer [Fig. 1(c)]. This six-atom cluster derived from the combined structures of  $\text{YSr}_2\text{Cu}_3\text{O}_{7+\delta}$ ,  $\text{YSr}_2\text{Cu}_{2.75}\text{Mo}_{0.25}\text{O}_{7.54}$ , and  $\text{YBa}_2\text{Cu}_3\text{O}_8$  now contains most of the functionality of the cuprates and enables our elucidation of the couplings between them. Our calculations show that, under certain conditions, the addition of the planar site,  $\text{O}_{\text{pl}}$ , and a soft, molecular  $\text{O}_{\text{ap}}\text{-Sr-O}_{\text{ap}}$  mode causes the double-well potential of the  $\text{O}_{\text{ap}}$  positions in the three-atom cluster [Fig. 1(d)] to enlarge to a triple well that now involves the  $\text{O}_{\text{pl}}$  [Fig. 1(e)], where the depth of the middle well is controlled by the Sr-related anharmonicity.

Our six-atom cluster has been evaluated from four different perspectives. First, we exactly diagonalized the associated quantum many-body Hamiltonian incorporating these additional structural ingredients. We find that the anharmonicity related to the unusual dynamical structure observed in the EXAFS spectrum of Sr/Ba-based cuprates [41,42] is due to its vicinity to a first-order synchronization transition of the IQTPs correlated with the two-site Cu(2)- $\text{O}_{\text{ap}}$  pair distribution. Second is the realization that an advantageous approach to what is now effectively a system of oscillators is adapting the Kuramoto treatment of networks [43], which has not previously been attempted in a crystal because of the complex network of couplings through the multiplicity of phonons and because it is an application to a quantum system. In order

to provide physical meaning to such a first-order transition, we mapped the combined, linearized Heisenberg equations of motion for the anharmonically coupled phonons to a mean-field Kuramoto equation describing the synchronization of IQTPs within the cluster. The mapping includes both the IQTP anharmonic coupling as well as temperature/dissipation (through thermal disorder) and yields a first-order synchronization transition to the antiphase motions of the two IQTPs. Surprisingly, we find that in the synchronized phase charge is pumped from the apical positions into the conducting CuO<sub>2</sub> plane while, simultaneously, a Sr-related, triatomic molecular vibration develops a finite projection also in the copper oxide plane. This is a novel planar IQTP, associated with Cu-O<sub>pl</sub> deformations. Third, we have confirmed the numerical results by performing a multimodal, nonlinear Bogoliubov transformation and demonstrated a polaronic degree of freedom associated with the coupling between excess charge in the plane and a new, anharmonicity-related, lattice vibration. Finally, we have observed that all of our theoretical and numerical results can be summarized in terms of an effective quantum-mechanical triple-potential-well model [Fig. 1(e)]. This represents an anharmonic structural adiabatic passage (ASAP) promoting antiphase IQTP synchronization and internal charge transfer.

The paper is organized as follows: In Sec. II we describe the here proposed extension of the three-atom into the six-atom cluster and the numerical methodology used to diagonalize its Hamiltonian. In Sec. III the numerical results are presented and discussed within the approach of the Kuramoto model for synchronization of the IQTPs; we present the nonlinear multimodal Bogoliubov transformation and the triple-well interpretation. Finally, Sec. IV is devoted to the conclusions.

## II. EXACT DIAGONALIZATION

We started by performing the exact diagonalization for the extended 6-atom cluster shown in Fig. 1(c). As discussed previously, the cluster was carefully chosen to include two important structural ingredients: (i) a Cu-O<sub>pl</sub>-Cu charge transfer bridge, associated with a nearby, planar oxygen (O<sub>pl</sub>) atom, promoting the transfer of the extra hole and longer Cu-O<sub>ap</sub> distance between the two lateral Cu-O<sub>ap</sub> IQTPs through the CuO<sub>2</sub> plane; and (ii) an O<sub>ap</sub>-Sr-O<sub>ap</sub> triatomic molecule, associated with a nearby Sr atom, promoting the anharmonic coupling, referred to as  $K$ , between the apical oxygens locations of the two lateral Cu-O<sub>ap</sub> IQTPs through the non-charge-transfer Sr atom. Notice that while the transfer included in (i) favors charge delocalization, the formation of a triatomic molecule, included in (ii), favors the locking of the phases of vibration above a critical anharmonicity  $K_c$ . As a result of the above rich structure, it is natural to expect that, as anharmonicity is fine tuned across the cluster, regimes where the excess charge becomes delocalized and vibrations become synchronized are not only to be expected, but, as we are about to show, remarkably interconnected. This process ultimately provides meaning to the anharmonicity-related data observed in EX-AFS as discussed previously.

The intricate interplay between lattice and charge degrees of freedom described above can be captured by the following

Hamiltonian  $H = H_{\text{el}} + H_{\text{ph}} + H_{\text{el-ph}} + H_{\text{Sr}}$  composed of four terms

$$H_{\text{el}} = \sum_i \varepsilon_i n_i + t \sum_{\langle ij \rangle \sigma} c_{i\sigma}^\dagger c_{j\sigma} + \text{H.c.} + U \sum_i n_{i\uparrow} n_{i\downarrow}, \quad (1)$$

$$H_{\text{ph}} = \hbar\omega b_L^\dagger b_L + \hbar\omega b_R^\dagger b_R, \quad (2)$$

$$H_{\text{el-ph}} = \lambda n_L (b_L^\dagger + b_L) + \lambda n_R (b_R^\dagger + b_R), \quad (3)$$

$$H_{\text{Sr}} = \hbar\Omega_{\text{Sr}} \beta^\dagger \beta + K (\beta^\dagger b_L b_R + \beta b_L^\dagger b_R^\dagger). \quad (4)$$

In the electronic part Eq. (1),  $c_{i,\sigma}^\dagger$ ,  $c_{i,\sigma}$  are the usual creation and annihilation operators for holes with spin projection  $\sigma$ , with  $i = 1, \dots, 5$  representing the O<sub>ap</sub>-Cu-O<sub>pl</sub>-Cu-O<sub>ap</sub> charger transfer sites, respectively,  $n_i = \sum_\sigma c_{i,\sigma}^\dagger c_{i,\sigma}$  is the number occupation operator for holes at sites  $i$ , where  $n_1 = n_L$  and  $n_5 = n_R$ , with on-site energies  $\varepsilon_i$ ,  $t$  is the spin-preserving, nearest-neighbor hopping amplitude, and  $U$  the on-site Coulomb repulsion to prevent double occupancy. The site energies were chosen so that out of a total of three holes, as considered in this work, two of them will always be favored at the two Cu atomic positions, while only a single, remaining excess hole minimizes the total energy by moving among the oxygen atoms while avoiding the two copper atomic positions. The phonon part Eq. (2) consists of the two harmonic infrared oscillators, of identical normal frequencies  $\omega$  whose creation and annihilation operators  $b_L^\dagger$ ,  $b_L$  and  $b_R^\dagger$ ,  $b_R$  represent the two possible lateral Cu-O<sub>ap</sub> positions, to the left (L) and to the right (R), in the cluster. The electron-phonon interaction term Eq. (3) describes the local coupling between the hole degrees of freedom to the lattice displacements, controlled by the coupling constant  $\lambda$ . This type of local electron-phonon coupling (Holstein model) is chosen due to its simplicity compared to nonlocal couplings (Su-Schrieffer-Heeger model) and because the same physical picture underlies the formation of a single polaron in the two cases [44]. The novelty here is Eq. (4), which was designed to provide the cluster with a nontrivial, O<sub>ap</sub>-Sr-O<sub>ap</sub> triatomic molecule structure, motivated by the coupling of the anharmonicity of the neighboring Sr to the behavior of O<sub>ap</sub> atoms and the superconductivity. To describe the normal modes of vibration of the triatomic molecule we have introduced creation (annihilation) operators  $\beta^\dagger$  ( $\beta$ ) for a moderately stiff harmonic molecular phonon of normal frequency,  $\Omega_{\text{Sr}} = 2\omega$ , as required by energy conservation. As we can see from Eq. (4) the new interaction term between the molecular phonons and the rest of the cluster is indeed anharmonic, in the form of a three-phonon coupling, and controlled by an anharmonic coupling,  $K$ . This interaction term can be interpreted as a molecule formation term, and  $K$  as a chemical potential that controls processes in which left and right phonons are destroyed to form a molecular mode,  $\beta^\dagger b_L b_R$ , as well as a destruction of a molecular vibration to produce left and right independent oscillations,  $\beta b_L^\dagger b_R^\dagger$ . As such, one would naturally expect that a molecule formation interaction would work toward promoting the locking of phases for the O<sub>ap</sub> vibrations, or equivalently, the synchronization of Kuramoto oscillators. For this reason the anharmonic coupling,  $K$ , will be referred to as the Kuramoto coupling.

The exact diagonalization of the full Hamiltonian, for the ground and excited states, was performed using a basis of

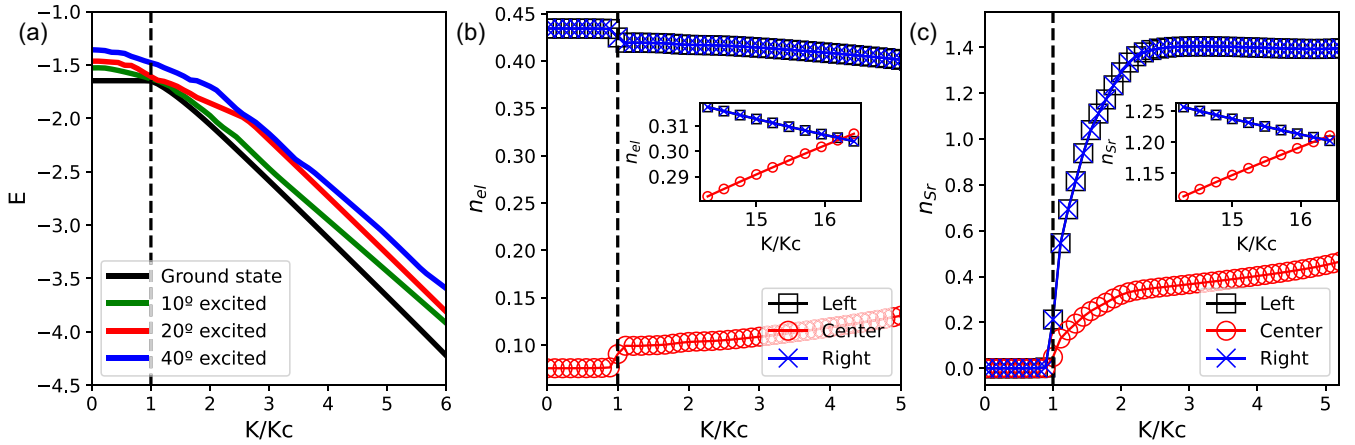


FIG. 2. (a) The ground state energy of the 6-atom cluster Hamiltonian as a function of reduced anharmonicity,  $K/K_c$ , for the nonadiabatic, intermediate  $\lambda$  coupling regime where lateral polarons are already formed: ground state (black), 10th excited state (green), 20th excited state (red), 40th excited state (blue). (b) The electronic occupations for left/right  $O_{ap}$  (black/blue squares/crosses) as well as for the central  $O_{pl}$  (red circles), as a function of reduced anharmonicity,  $K/K_c$ , of the ground state. (c) The phonon occupations for left/right sites (black/blue square/cross) as well as for the central oxygen site (red circles), as a function of reduced  $K/K_c$  anharmonicity, of the ground state. Insets: As we increase anharmonicity, the central electronic (b) and phonon (c) occupations surpass the lateral ones.

wave functions given by

$$|\Psi\rangle = \sum_{i,\gamma,\beta,\delta} \alpha_{i\gamma\beta\delta} |n_i\rangle |n_\gamma\rangle |n_\beta\rangle |n_\delta\rangle, \quad (5)$$

corresponding to an  $n_{el} \times n_L \times n_R \times n_{Sr}$  dimensional Hilbert space. For the electronic states  $|n_i\rangle$  we first considered all possible spin-up and spin-down configurations at the five charge transfer sites and a total of three holes added to the cluster. However, as discussed above, since only a single (excess) hole is found over the five charge transfer sites while the other two are favored at the copper sites, our electronic subspace was limited to  $n_{el} = 28$  states. The bosonic  $|n_\gamma\rangle |n_\beta\rangle |n_\delta\rangle$  states represents the phonon degrees of freedom for the left and right apical positions and for the Sr-related triatomic molecule, respectively. These states were written in a bosonic occupation number representation for a total of  $n_L = n_R = n_{Sr} = 5$ , justified by continuously enlarging the phonon Hilbert subspace, through a systematic increase of the number of phonon modes until convergence.

For the numerical parameters in the Hamiltonian (1)–(4) we used [23]  $\varepsilon_{1,3,5} = -\varepsilon_{2,4} = 0.5$  eV, favoring holes at the Cu atoms,  $t = 1.0$  eV, and  $U = 7.0$  eV. For the electron-phonon coupling, we set  $\lambda = 0.3$  eV, inside the nonadiabatic regime for polaron formation [45], and we have chosen the stiff, triatomic molecule frequency,  $\Omega_{Sr} = 0.12$  eV, to be precisely twice the value of  $\omega = 0.06$  eV, as required by energy conservation.

### III. NUMERICAL RESULTS AND DISCUSSION

In Fig. 2 we summarize the results obtained from our numerical, exact diagonalization studies. Figure 2(a) shows the ground and three representative excited state energies as a function of the reduced coupling,  $K/K_c$ . For the ground state (black line; first from bottom up) one observes a clear kink at  $K/K_c = 1$  while for all higher excited states (green, red, and blue lines; second, third, and fourth from bottom up) there is

no clear kink, although a decrease in energy is evident even for  $K < K_c$ . We can see that for the higher excited states, the definition of a critical coupling is not as clear as for the ground state because of level avoiding behavior. Since higher excited states will play a significant role only when  $T \neq 0$ , we restrict ourselves to the behavior of the ground state across the synchronization transition. Figure 2(b) shows the electronic occupations at the left (black squares), central (red circles), and right (blue crosses) sites, also as a function of the reduced coupling,  $K/K_c$ , for the ground state. At the critical coupling,  $K_c$ , we have found a delocalization transition of the excess hole, as anticipated. In fact, while prior to the transition the hole wave function had weight only at either the left or right apical oxygen atoms, indicating formation of localized polarons, above  $K_c$  the electronic occupation for the central (planar) oxygen atom begins to increase monotonically while both the left and right occupations decrease. Indeed, when  $K \gg K_c$ , the central occupation is greater than the apical ones. The abrupt discontinuity demonstrates that the phase transition is first order and this behavior indicates the formation of a *split polaron*. Finally, Fig. 2(c) shows the occupations of Sr-related, molecular phonons at the left (black squares), right (blue crosses), and central (red circles) positions within the cluster. When  $K$  crosses  $K_c$ , all phonon modes related to the triatomic molecule become active, which is expected from the apical oxygens' phase locking driven by the synchronization. But remarkably, as shown in the inset, the increase of anharmonicity drives the central projection of molecular phonons to be greater than the lateral ones.

The numerical results reveal three important features associated with the Hamiltonian (1)–(4) as anharmonicity, encoded in the Kuramoto parameter  $K$ , is varied, Fig. 3: (i) As shown in Sec. III A, it produces a first-order synchronization phase transition associated with the anharmonicity-related, triatomic molecular locking or synchronization of the phases of vibration corresponding to the two  $O_{ap}$  locations or Cu- $O_{ap}$  distances when the Kuramoto coupling  $K$  is increased,



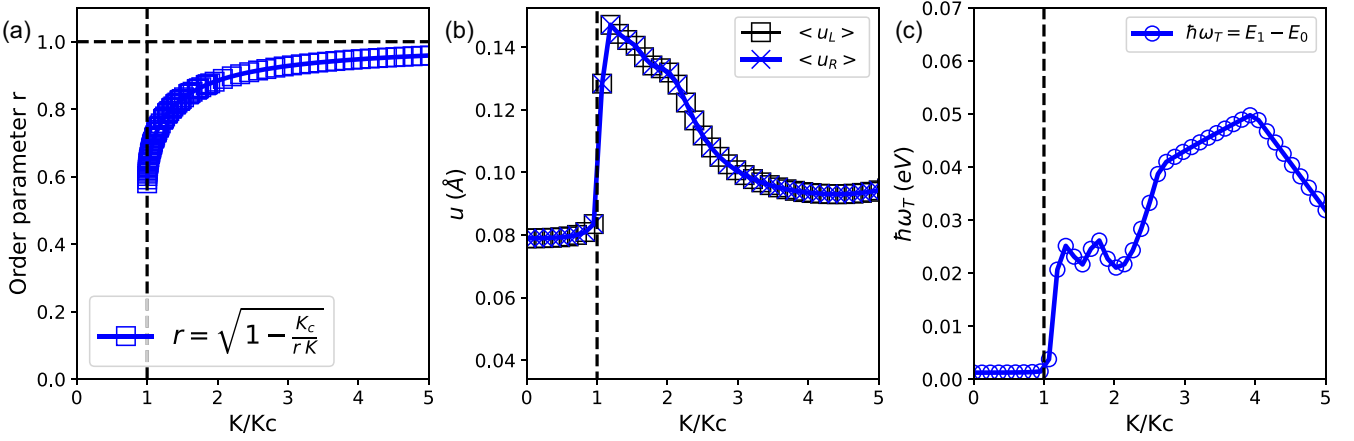


FIG. 3. (a) The solution to Kuramoto's order parameter Eq. (7) as a function of the reduced coupling in the ground state, showing a first-order synchronization phase transition. (b) Displacement  $\langle u \rangle = \sqrt{\hbar}/2m\omega(b + b^\dagger)$  of the  $O_{ap}$  equilibrium position for both the left and right positions in the cluster. (c) The polaronic tunneling frequency.

evidenced by the evolution of the Kuramoto order parameter,  $r$ , with anharmonicity [Fig. 3(a)]. (ii) The second is a nonlinear behavior for the displacement  $\langle u \rangle$  related to the apical oxygens, which is quantitatively in agreement with the experimental deviations found in the two-site distributions associated with the Cu- $O_{ap}$  pairs [46] [Fig. 3(b)]. Before the transition, there is a stable  $|\langle u \rangle| \approx 0.08$  Å position, since  $\lambda$  is strong enough to form localized, frozen polarons, and although a dynamical shift occurs after the synchronization (a signature of the nonlinear behavior), there is still agreement with EXAFS measurements of the distance in the Cu- $O_{ap}$  pair [45]. (iii) It generates a polaronic tunneling frequency,  $\hbar\omega_T = E_1 - E_0$ , that is the difference in energy from the first to the ground state [22], that evolves nontrivially with  $K$  [Fig. 3(c)]. There is a jump at the critical coupling, indicating the value of the anharmonicity beyond which the initially frozen polarons become an IQTP, allowing quantum tunnel internally between the two lateral positions in the cluster. In order to address each one of these issues, we proceed by applying three different techniques.

### A. The first-order synchronization phase transition

Collective behavior and its spontaneous emergence in networks of coupled oscillators is a common characteristic in many systems across science, and perhaps the simplest model that describes the synchronization phenomena is the Kuramoto model [47]. Its application ranges from classical systems in physics [48] and biology [49] to quantum physical systems [50–52]. The Kuramoto model is based on two properties: the node oscillators are coupled via a superfluid density  $K_{ij}$  and there are white, quenched,  $\delta$  or thermal,  $k_B T$ , noises that are present due to the environment the networks are embedded in. Synchronization can be achieved whenever the couplings predominate over the noises. The synchronization process is described by a complex order parameter,  $re^{i\psi}$ , where the real part  $r$  sets the character of the synchronization:  $r = 0$  for the unsynchronized phase,  $0 < r < 1$  for partial, and  $r = 1$  for full synchronization [see Fig. 3(a)]. The phase  $\psi$  in the imaginary part of the order parameter sets the overall phase that the oscillators achieve when synchronized.

As demonstrated in Appendix A, the set of coupled equations of motion for the vibrational degrees of freedom obtained from the Hamiltonian (1)–(4) can be conveniently rewritten, within a mean-field approximation [52,53], as a single, first-order differential equation for the phases of the lateral oscillators,  $\theta_i$ , in which temperature effects can be added by introducing a white thermal noise,  $\zeta_i(t)$ , thus providing, in terms of the Kuramoto complex order parameter  $re^{i\psi}$ ,

$$\dot{\theta}_i = \omega_i + Kr^2 \sin[\theta_i(t) + \psi] + \xi_i(t), \quad (6)$$

such that  $\langle \zeta_i(t) \rangle = 0$  and  $\langle \zeta_i(t)\zeta_j(t') \rangle = 2\gamma k_B T \delta_{ij} \delta(t - t')$ , where  $\gamma$  is a damping constant. The solution to such first-order equations yields

$$r = \sqrt{1 - \frac{K_c(\delta, T)}{rK}}, \quad (7)$$

unveiling the connection between the Kuramoto order parameter and the anharmonicity introduced in the cluster. It also shows the first-order nature of the synchronization transition that occurs at  $K_c(\delta, T)$ , a critical coupling [see Eq. (A10)] that is determined both by the temperature  $T$  as well as a quenched spread  $\delta$  that relates to disorder. In summary, the process of increasing anharmonicity induces the localized polaronic phase ( $K < K_c$ ) to evolve into a phase of synchronized internal tunneling polarons, since  $\hbar\omega_T \neq 0$  for  $K > K_c$  [Fig. 3(c)], changing dynamically the otherwise stable position of the Cu- $O_{ap}$  pairs [Fig. 3(b)].

### B. The formation of a planar IQTP

The exact diagonalization results show that not only the total Sr-phonon occupation jumps at  $K_c$  but also, most interestingly, an unexpected Sr-phonon central occupation,  $n_\beta(C)$ , appears above the first-order antiphase synchronization transition. This observation motivated us to *break down* the  $O_{ap}$ -Sr- $O_{ap}$  triatomic molecule term of the original Hamiltonian (4) as

$$H_{Sr} = \sum_r \hbar\Omega_{Sr} \beta_r^\dagger \beta_r + K \sum_r (\beta_r^\dagger b_L b_R + \beta_r b_L^\dagger b_R^\dagger), \quad (8)$$

where  $\beta_r, \beta_r^\dagger$  are now to be understood as the projection of the triatomic molecular vibration at the relevant sites of the cluster, namely  $r = L, C, R$ .

In order to diagonalize the Hamiltonian and connect the numerical results showing the appearance of an excess charge, together with phonon projections in the central, planar site of the cluster, which leads to the formation of a planar IQTP, we introduce a nonlinear, multimodal Bogoliubov transformation for the lateral phonons as

$$b_L = \sum_r (u_{L,r}^* \beta_r B_r + v_{L,r} \beta_r^\dagger B_r^\dagger), \quad r = R, C, \quad (9)$$

$$b_R = \sum_r (u_{R,r} \beta_r^\dagger B_r^\dagger + v_{R,r}^* \beta_r B_r), \quad r = L, C, \quad (10)$$

together with the complex conjugate  $b_L^\dagger$  and  $b_R^\dagger$ . We emphasize that by transforming the Hamiltonian from the lateral phonon operators to the new bosonic  $B_r$  modes, we are searching for the limit where the charge and phonon projections at the central site ( $r = C$ ) are interacting. This is achieved by taking the limit of strong anharmonicity  $K \gg K_c$ , as suggested by the numerical results in the insets of Fig. 2(b) and Fig. 2(c). Therefore, after applying the Bogoliubov transformation procedure in this limit (see Appendix B), the total diagonal phonon Hamiltonian in terms of new Bogoliubov phonons can be written as

$$H'_d = \hbar F(K) B_C^\dagger B_C, \quad (11)$$

and anharmonicity-dependent, novel, central phonon modes are present, whose natural frequencies  $\hbar F(K)$  are given by

$$\hbar F(K) = \frac{\hbar\omega}{A\gamma} \{ \omega[1 + 2n_\beta(C)] - \gamma \} + \frac{K\sqrt{n_\beta(C)}}{A\gamma} \sqrt{\omega^2 - \gamma^2} [1 + 2n_\beta(C)], \quad (12)$$

where  $n_\beta(C)$  is the occupation of Sr-related triatomic molecular phonons projected on the central site [red circles in Fig. 2(c)],  $\hbar\gamma = \sqrt{(\hbar\omega)^2 - K^2 n_\beta(C)}$ , and  $A = 1 + n_\beta(C) + n_B(C)$ . We have found that, before synchronization,  $K < K_c$ ,  $\hbar F(K) = 0$  because  $n_\beta(C) = 0$ ; thus these new phonon modes are only present in the limit of strong anharmonicity  $K \gg K_c$ . The multimodal, nonlinear Bogoliubov transformation needs also to be applied to the original electron-phonon coupling, which together with Eq. (11), gives rise to the new transformed Hamiltonian, that can be written as

$$H'_{Sr} = \hbar F(K) B_C^\dagger B_C + \lambda' n_{ap} (B_C + B_C^\dagger), \quad (13)$$

where  $n_{ap}$  is to be understood as the electronic occupation at the apical positions and the new excess-hole-central-phonon coupling is given by

$$\lambda' = \frac{2\lambda\sqrt{n_\beta(C)}}{\sqrt{2A\gamma}} (\sqrt{\omega + \gamma} + \sqrt{\omega - \gamma}). \quad (14)$$

This is a striking result and demonstrates that after the synchronization of the left and right  $O_{ap}$  vibrations, the transition to a synchronized IQTP phase, with the pumping of charge and phonon projection to the  $\text{CuO}_2$  plane, promotes the formation of an IQTP in the central, planar

site, as suggested by the numerical results. Therefore, our analysis has demonstrated that a planar IQTP arises from the synchronization transition, providing theoretical support to the observation of IQTPs in the planar oxygen ( $O_{pl}$ ) of the  $\text{CuO}_2$  planes in some compounds [25–32], and even in other high-temperature superconductivity (HTSC) materials [33–35].

The electron-phonon part,  $H'_{el-ph}$ , of the transformed Hamiltonian, the second term in Eq. (13), can also be written in a way to show the explicit interaction between the central electronic occupation and the new phonon modes present at the same site. Since only one excess hole is added to the system, the constraint  $n_L + n_R + n_C = 1$ , or even  $2n_{ap} + n_C = 1$ , is valid, and thus  $n_{ap} = (1 - n_C)/2$ . Therefore, the Bogoliubov analysis supports the interpretation of the triple-well structure arising after the IQTPs synchronize, which we explore in the next section.

### C. The triple well

The triple-well structure can now be elucidated. Before synchronization,  $K < K_c$ , we have  $n_\beta(C) = 0$  and  $n_{el}(C) = 0$ ; thus the system contains two decoupled harmonic vibrations localized at each possible  $L, R$  position, composing a double-well structure [see Fig. 4(a)]. The potential depth and width are large and the symmetric and antisymmetric components of the lateral ground state wave function are degenerate, while a central excited state is too energetic to support tunneling. In this case the single excess hole in the cluster is found either at the (L) or (R) apical oxygen atoms. Once the system is prepared at the (L) position, for example, it remains at that position even after time evolves, as shown explicitly in Fig. 4(b). This results from the absence of a tunneling frequency for  $K < K_c$  as shown in Fig. 3(c). The ground state wave function coefficients given in Fig. 4(c) show the polaron localization as finite occupation appears only at the lateral positions, and zero electronic occupation at the central position, for  $K < K_c$ .

After synchronization,  $K > K_c$ , however, we have  $n_\beta(C) \neq 0$  and  $n_{el}(C) \neq 0$ . The central site of the system is now active, and when  $K \gg K_c$  a new harmonic central phonon mode is present, composing a three-well structure as shown in Fig. 4(d). The symmetric and antisymmetric solutions of the wave function become nondegenerate and the central well on the planar oxygen site in the synchronized phase substantially lowers the energy of the excited state, forming an ASAP that promotes tunneling between left and right IQTPs. This results in the nonzero tunneling frequency of the synchronized phase. In this case the single excess hole in the cluster can be found at all (L), (R), and (C) oxygen atoms. If the system is prepared at the (L) position the existence of a finite tunneling frequency shows that the wave function evolves with time and the excess hole becomes delocalized. This is depicted in Fig. 4(e). The ground state wave function coefficients given in Fig. 4(f) shows finite but decreasing occupations at the lateral positions, and nonzero, increasing electronic occupation at the central position, for  $K > K_c$ . Small but finite occupation of the excess hole also occurs on the two Cu sites, demonstrating delocalization throughout the entire cluster.

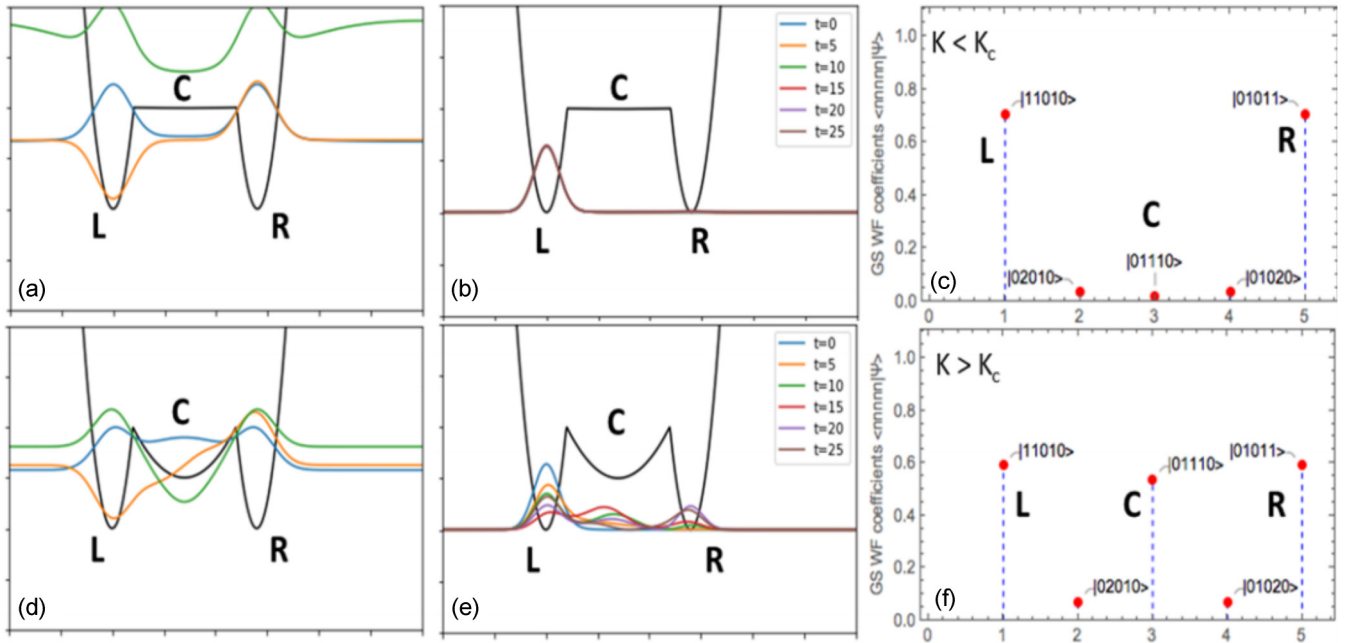


FIG. 4. (a) For  $K < K_c$ , the potential (black) depth, the symmetric (blue) and antisymmetric (orange) components of the lateral ground state wave function, and a central excited state (green). (b) The absence of tunneling of the polarons in this scenario is demonstrated by its fixed position over time. (c) Ground state wave function coefficients for the unsynchronized, localized polaron phase. (d) for  $K > K_c$ , the triple-well potential (black), the symmetric (blue) and antisymmetric (orange) solutions of the wave function, and the excited state (green). (e) Due to the ASAP, the IQTP is now observed to tunnel from left to right through the center as time evolves. (f) Ground state wave function coefficients for the synchronized IQTP phase. The states in (c) and (f) are represented in the electronic occupation representation for the three holes in the five charge transfer sites.

#### IV. CONCLUSION

Our exact diagonalization calculations of the original 3-atom O-Cu-O cluster produced significant but limited results on experimental signatures of IQTPs [16,17,21]. In this work, we have expanded the cluster to 6 atoms to incorporate the essential functionalities of the layered cuprate structures: a pair of Cu-O<sub>ap</sub> IQTPs, their O<sub>pl</sub> bridge that adds the CuO<sub>2</sub> conducting planes, and their divalent alkaline earth cation (Sr) that, with the O<sub>ap</sub> atoms, completes the atoms of the dielectric layer. This extension allows a much more detailed investigation of the local interplay between the lattice and electronic degrees of freedom in the cuprates and related compounds. A novel and crucial element in these calculations is the anharmonic, three-phonon coupling in the cluster Hamiltonian whose character and coupling to the superconductivity has been identified by EXAFS measurements on several compounds [37,42,46]. The most notable result reported in this work, that should be generalized beyond cuprates to related systems, is the transition to a synchronized phase whose broken symmetry is found in the dynamic structure. This occurs at a critical anharmonic coupling,  $K_c$ , the Kuramoto coupling between the two IQTPs. Pertinent to the electron-lattice coupling and possible associated superconductivity mechanism in this spontaneous heterostructure is that in the synchronized phase a fraction of the excess charge that was originally localized as small polarons frozen on the O<sub>ap</sub> is transferred to the O<sub>pl</sub> of the CuO<sub>2</sub> planes that are the locations of the superconductivity in the oxide cuprates. A second relevant behavior of the synchro-

nized phase is the projection from the triatomic O<sub>ap</sub>-Sr-O<sub>ap</sub> molecule of phonon modes throughout the cluster. These are controlled by the new phonon ( $\beta$ ) in the anharmonic term of the Hamiltonian. The displacements of the O<sub>ap</sub> atoms from their static positions to form the two-site distribution,  $\langle u \rangle$ , quantitatively reproduce the 0.12–0.2 Å separations found by EXAFS [46]. This agreement with experiments supports our calculations.

Furthermore, here the Kuramoto model was applied by mapping the Heisenberg equations of motion for each oscillator in the O<sub>ap</sub> position to a system of coupled oscillators. By doing so we could describe the transition at  $K_c$  as an antiphase synchronization transition for the phases of each lateral oscillator. For  $K > K_c$ , the otherwise localized polarons, or independent vibrations, became dynamically active in the form of synchronized IQTPs due to the presence of the stiff molecular vibration brought by the Sr atom in the cluster that connects the two Cu-O<sub>ap</sub> pairs. Moreover, a nonlinear Bogoliubov transformation was applied to the Hamiltonian in a way that, in the limit of strong anharmonicity,  $K \gg K_c$ , new phonon modes are present in the planar site. In combination with excess charge pumped into the O<sub>pl</sub> of the CuO<sub>2</sub> plane in the synchronized IQTP phase, a new electron-phonon, thus a polaronic, degree of freedom occurs in the plane that can be interpreted as a planar IQTP [25–32]. Together, these theoretical findings point to the triple-well potential interpretation, where the appearance of a finite tunneling frequency in the synchronized phase originates in the pumping of charge from O<sub>ap</sub> onto the O<sub>pl</sub> site. This lowers the energy of this site and enables the excess charge to quantum tunnel across the cluster,

resulting in the internal quantum tunneling polaron dynamics of the system.

Despite the limitations inherent to the small 6-atom cluster, we emphasize that the additional components of this larger cluster and especially the anharmonicity introduced by the Sr atom [41,42] are crucial to understanding the dynamics of lattice and charge degrees of freedom in this system. This points toward the need to understand how anharmonic phonons can influence important characteristics of different systems [54–56], now including cuprates. In this work, we have added a new interpretation of the dynamics related to the collective motion of atoms in the lattice based on the Kuramoto model for synchronization. These results motivate further investigation of the connection between synchronized IQTPs described as Kuramoto oscillators and anharmonic phonons and its role in the charge-lattice dynamics of cuprates, including superconducting properties and the role of Coulomb repulsion, as for example when considering two holes added in an IQTP or the patterning of finite densities of coupled IQTPs [57]. We note that EXAFS measurements of cuprates in which Co, Mn, and Ni were substituted for a fraction of the Cu in the CuO<sub>2</sub> planes demonstrated that the Cu-O IQTPs are not only coupled to but in fact play a direct role in HTSC [36]. Recent reports on highly overdoped superconducting cuprates prepared by high-pressure oxygen (HPO) methods have provided exceptions to many of what have been considered common unifying behaviors of cuprate superconductivity, namely, in Sr<sub>2</sub>CuO<sub>3,3</sub>, copper oxide planes as CuO<sub>1.5</sub> instead of CuO<sub>2</sub> [37]; continued retention of or increases in  $T_c$  throughout their 50–115 K transition temperatures through excess Cu charge values even beyond 0.6, which far exceed the 0.27 limit of the dome in the conventional phase diagram [46]; a reversal of the correlation between longer Cu-O<sub>ap</sub> distances and higher  $T_c$ , oblate Cu geometry, and inversion of the Cu  $3d_{z^2-r^2}$  and  $3d_{x^2-y^2}$  energies in Ba<sub>2</sub>CuO<sub>3,2</sub> [58]; and a structural transformation concomitant with the superconducting transition [59]. Insofar as a universal factor is the presence of IQTPs coupled to the superconductivity, our findings on IQTP signatures in the dynamic structure may play a key role in developing the still unresolved HTSC pairing and condensation mechanism.

#### ACKNOWLEDGMENTS

The authors acknowledge the financial support from the Slovenian Research Agency (Core Funding No. P1-0040). Work at Washington State University is partially supported by the U.S. National Science Foundation, Division of Materials Research, Early Concept Grants for Exploratory Research, Grant No. 1928874. Use of the Stanford Synchrotron Radiation Lightsource, SLAC National Accelerator Laboratory, is supported by the U.S. Department of Energy, Office of Science, Office of Basic Energy Sciences, Contract No. DE-AC02-76SF00515. V.V. and M.B.S.N. acknowledge the financial support of CAPES and FAPERJ.

#### APPENDIX A: KURAMOTO'S SYNCHRONIZATION TRANSITION

We start by providing meaning to the first-order transition. To this end, we shall make use of a mean-field approximation

to treat the anharmonic three-phonon term in Eq. (4). For convenience, first we rescale the anharmonic coupling  $K \rightarrow K/N$ , where  $N$  represents the number of different oscillators (phonons) at each of the two kinds of oscillator communities: left (L) and right (R) oscillators. Second, since all oscillators are bosons we introduce a mean-field approximation in terms of which the triatomic molecular phonon population can be written as  $\langle \beta^\dagger \beta \rangle = |R|^2 = \langle \beta^\dagger \rangle \langle \beta \rangle = R^* R \neq 0$ , where  $R$  plays the role of a complex order parameter. Now, the Heisenberg equations of motion derived from Hamiltonian (1)–(4) for  $i = L, R$  phonons read

$$\begin{aligned} i \frac{db_i}{dt} &= \omega_i \left( b_i - \frac{\lambda n_i}{\hbar \omega} \right) + \frac{KR}{N\hbar} b_j^\dagger, \\ -i \frac{db_i^\dagger}{dt} &= \omega_i \left( b_i^\dagger - \frac{\lambda n_i}{\hbar \omega} \right) + \frac{KR^*}{N\hbar} b_j. \end{aligned} \quad (\text{A1})$$

So far, this is a set of coupled operatorial differential equations. Let us take the quantum mechanical expectation value at both sides of the above equations, and recall that phonon coherent states are eigenstates of the annihilation operator  $b_{i,j}|z_{i,j}\rangle = z_{i,j}|z_{i,j}\rangle$ . We then drop all constant terms that simply provide an overall shift of the equilibrium position and write the complex numbers  $z_{i,j} = z_0 e^{-i\theta_{i,j}(t)}$ , where we have made the assumption that the amplitudes of the phonons L and R are equal,  $z_0$ , and only their phases change. Finally we introduce Kuramoto's complex order parameter,  $R = r e^{i\psi}$ , where  $r$  is the real part of  $R$  and  $\psi$  is an arbitrary phase. Furthermore, we choose  $R = -ir$ , as purely imaginary, so that after combining the two equations in (A1) we arrive at

$$\frac{d\theta_i(t)}{dt} = \omega_i + \sum_{j=L,R} \frac{Kr}{N\hbar} \sin[\theta_i(t) + \theta_j(t)]. \quad (\text{A2})$$

We recognize the dynamical problem in (A2) as a Kuramoto differential equation for antiphase synchronization  $\theta_i \rightarrow -\theta_j$ . The mean-field version of the above equation is obtained as usual, by introducing the order parameter [43]  $r e^{i\psi} = 1/N \sum_{j=1}^N e^{i\theta_j}$ . Here the real part  $r$  plays the role of the coherence amplitude for a population of  $N$  phase oscillators and  $\psi$  indicates the coherence phase. Kuramoto's mean-field equation can then finally be written as

$$\dot{\theta}_i(t) = \omega_i + Kr^2 \sin[\theta_i(t) + \psi], \quad (\text{A3})$$

where from now on we set  $\hbar = 1$ . According to Eq. (A3), phase locking occurs for  $\theta_i \rightarrow -\psi$ , and as such the antiphase synchronization favored by Eq. (A2) implies  $\theta_j \rightarrow \psi$ . Now, since we have chosen before  $\psi = -\pi/2$  (such that  $R = r e^{i\psi} = -ir$ ) we end up with  $\theta_i + \theta_j = 0$  and  $\theta_i - \theta_j = -\pi$ , which reflects the antiphase synchronization transition.

Once we established the antiphase character of the synchronization transition, we now show its first-order nature. For that, the mean-field analysis initiated above for the Kuramoto model needs to be supplemented by a self-consistent equation [43] such as

$$1 = Kr \int_{-\frac{\pi}{2}}^{\frac{\pi}{2}} \cos^2 \theta g(Kr^2 \sin \theta) d\theta, \quad (\text{A4})$$



where  $g(\omega)$  is a symmetric Lorentzian distribution of frequencies with quenched spread  $\delta$  given by

$$g(\omega) = \frac{1}{\pi} \frac{\delta}{\omega^2 + \delta^2}. \quad (\text{A5})$$

Solving the self-consistent equation, one finds for the order parameter

$$r = \sqrt{1 - \frac{K_c(\delta)}{K_r}}, \quad (\text{A6})$$

where  $K_c(\delta) = 2\delta$  is the critical coupling in terms of a quenched spread  $\delta$ .

Finally, since we would like also to incorporate thermal effects to the synchronization transition, we recall that temperature effects can be added to the problem by introducing a thermal noise

$$\dot{\theta}_i(t) = \omega_i + Kr^2 \sin[\theta_i(t) + \psi] + \xi_i(t), \quad (\text{A7})$$

such that  $\langle \xi_i(t) \rangle = 0$  and  $\langle \xi_i(t) \xi_j(t') \rangle = 2\gamma k_B T \delta_{ij} \delta(t - t')$ , where  $\gamma$  is a damping constant. In this case, the oscillator probability density  $\rho$  must satisfy the nonlinear Fokker-Planck equation [43]

$$\begin{aligned} \frac{\partial \rho}{\partial t} &= D \frac{\partial^2 \rho}{\partial \theta^2} - \frac{\partial(v\rho)}{\partial \theta}, \\ v &= \omega + Kr^2 \sin[\theta_i(t) + \psi], \end{aligned} \quad (\text{A8})$$

where  $v$  is the drift velocity and with  $D(\Omega) = \gamma k_B T \Omega$  a diffusion coefficient. The solution to these coupled equations yields

$$r = \sqrt{1 - \frac{K_c(\delta, T)}{K_r}}, \quad (\text{A9})$$

and we see that the only difference from Eq. (A6) is in the critical coupling, which now reads

$$\frac{2}{K_c(\delta, T)} = \int_{-\infty}^{+\infty} d\Omega \frac{g(D(\Omega) + \omega)}{\Omega^2 + 1}. \quad (\text{A10})$$

One important conclusion is that by mapping the Heisenberg equations of motion of each lateral phonon community controlled by  $b_L$  and  $b_R$  into a Kuramoto equation of phase oscillators, we are able to connect the Kuramoto order parameter  $r$  with the anharmonicity introduced in the cluster,  $K$ , that controls the exchange of independent vibrations and locked, triatomic molecular vibrations related to the presence of the Sr atom in the dielectric layer. The collective behavior of IQTPs is caused by the synchronization of the phonon communities present in the Cu-O<sub>ap</sub> pairs. Furthermore, the overall effect of temperature (dissipation through thermal noise) is to increase the critical coupling  $K_c$  of the ground state, making it harder for the oscillators to synchronize. The temperature increases the spread in the Lorentzian probability distribution for the oscillators and this leads to an increase of the critical anharmonicity for synchronization. Also, temperature introduced in connection to dissipation enhances decoherence, which leads to an increase of the critical coupling for synchronization. Elevating the temperature does not alter the character of the synchronization transition; it remains first order.

## APPENDIX B: THE NONLINEAR MULTIMODAL BOGOLIUBOV TRANSFORMATION

The correlated, anharmonic phonon Hamiltonian (1)–(4) of the main text can be diagonalized by means of a multimodal, nonlinear Bogoliubov transformation. To this end we introduce new phonons  $B_r, B_r^\dagger$  that connect to the original ones through

$$b_L = \sum_r (u_{L,r}^* \beta_r B_r + v_{L,r} \beta_r^\dagger B_r^\dagger), \quad r = R, C, \quad (\text{B1})$$

$$b_R = \sum_r (u_{R,r} \beta_r^\dagger B_r^\dagger + v_{R,r}^* \beta_r B_r), \quad r = L, C. \quad (\text{B2})$$

It is important to emphasize that, while the original  $b_L, b_R$  phonons are restricted to the L, R sites only, here  $r$  is allowed to run over the other positions:  $R, C$  for the left phonons and  $L, C$  for the right ones. This is what provides the transformation with a multimodal character. The nonlinear aspect results from the presence of quadratic terms such as  $\beta_r B_r$ .

Unitarity of the Bogoliubov transformation guarantees that the original commutation relations are preserved. We started with L and R phonons only, satisfying the commutation relations

$$[b_r, b_{r'}^\dagger] = \delta_{r,r'}, \quad r, r' = L, R. \quad (\text{B3})$$

Let us consider the simpler case where  $r = r'$ , in which case  $[b_r, b_r^\dagger] = 1$ , and impose the bosonic commutation relations

$$[B_r, B_{r'}^\dagger] = \delta_{r,r'}, \quad (\text{B4})$$

$$[\beta_r, \beta_{r'}^\dagger] = \delta_{r,r'}, \quad (\text{B5})$$

and expectation values of all phonon operators

$$n_\beta(r) = \langle \beta_r^\dagger \beta_r \rangle, \quad (\text{B6})$$

$$n_B(r) = \langle B_r^\dagger B_r \rangle. \quad (\text{B7})$$

Using  $b_L$  and  $b_L^\dagger$ , for example, the unitarity of the transformation reduces to a sum rule

$$[b_L, b_L^\dagger] = \sum_r (|u_{L,r}|^2 - |v_{L,r}|^2) [1 + n_B(r) + n_\beta(r)] = 1,$$

with a similar result for the right phonons, taking  $L \rightarrow R$ . After performing the Bogoliubov transformation, substituting Eqs. (B1) and (B2) in the Hamiltonian, one has to eliminate the nonlinear, anharmonic interaction by setting to zero the equation for the off-diagonal Bogoliubov coefficients. Since we are interested in studying what happens in the central, planar site of the cluster, after the synchronization transition, we restrict the transformation to the coefficients  $u_{r,C}$  and  $v_{r,C}$ , neglecting contributions coming from combinations of left/right coefficients, such as  $u_{L,L}$  or  $v_{R,L}$ , for example. Therefore, the equation we have to eliminate from the off-diagonal elements takes the form

$$\sum_{r=L,R} \hbar \omega u_{rC} v_{rC} + \frac{K}{2} \sqrt{n_\beta(C)} (u_{rC} u_{-r,C} + v_{rC} v_{-r,C}) = 0.$$

At this point, a few approximations are in order. First, we use that  $v_{-r,C} = v_{r,C}^*$  and the same for the other Bogoliubov

coefficients. From the numerical results of the exact diagonalization, we know that the Sr-phonon occupation in the central position becomes greater than the lateral ones; thus we shall restrict our subsequent analysis to the strong anharmonicity case,  $K \gg K_c$ , and approximate

$$\langle \beta_r^\dagger \beta_r^\dagger \rangle \approx \langle \beta_r^\dagger \rangle \langle \beta_r^\dagger \rangle = \sqrt{n_\beta(C)} \sqrt{n_\beta(C)} \delta_{r,C} \delta_{r',C},$$

which is basically the same approximation we have already used when discussing Kuramoto's mean-field equation. Using these approximations, we are left with

$$\sum_r \left[ \hbar \omega_{r,C} v_{r,C} + \frac{K}{2} \sqrt{n_\beta(C)} (|v_{r,C}|^2 + |u_{r,C}|^2) \right] = 0.$$

Solving for the expression inside square brackets we obtain the Bogoliubov coefficients

$$\begin{aligned} u_{r,C} &= \frac{1}{\sqrt{A}} \left( \frac{\omega + \gamma}{2\gamma} \right)^{1/2}, \\ v_{r,C} &= \frac{1}{\sqrt{A}} \left( \frac{\omega - \gamma}{2\gamma} \right)^{1/2}, \end{aligned} \quad (\text{B8})$$

where  $\hbar\gamma = \sqrt{(\hbar\omega)^2 - K^2 n_\beta(C)}$  and  $A = 1 + n_\beta(C) + n_B(C)$ . We see that in this limit the coefficients are actually independent of  $r$ , enabling us to use only  $u_C$  and  $v_C$ . Now we are ready to write down the total diagonal phonon Hamiltonian in terms of the new Bogoliubov phonons by substitution of the transformation inside the diagonal, harmonic term of the Hamiltonian in Eq. (2) and retaining only the central contributions. This yields

$$H'_d = \hbar F(K) B_C^\dagger B_C, \quad (\text{B9})$$

where the natural frequencies  $\hbar F$  are given by the expression

$$\begin{aligned} \hbar F(K) &= \frac{\hbar\omega}{A\gamma} \{ \omega [1 + 2n_\beta(C)] - \gamma \} \\ &+ \frac{K \sqrt{n_\beta(C)}}{A\gamma} \sqrt{\omega^2 - \gamma^2} [1 + 2n_\beta(C)]. \end{aligned} \quad (\text{B10})$$

We can see that, before synchronization,  $K < K_c$ ,  $\hbar F = 0$ , because  $n_\beta(C) = 0$ , which is expected when compared with the numerical results shown in the main text; i.e., the new phonons are only present after the central site becomes activated by the synchronization of the IQTPs. We have to also consider the effect of the Bogoliubov transformation in the original electron-phonon coupling of the Hamiltonian in Eq. (3). In terms of the new phonon operators we have for  $b_L + b_L^\dagger$ , as an example,

$$\left\{ \sum_r (u_{L,r}^* \beta_r B_r + v_{L,r} \beta_r^\dagger B_r^\dagger) + \sum_r (u_{L,r} \beta_r^\dagger B_r^\dagger + v_{L,r}^* \beta_r B_r) \right\},$$

where by performing the same procedure we used for the diagonal, harmonic terms  $b_L^\dagger b_L$  and  $b_R^\dagger b_R$ , we write the transformed

electron-phonon Hamiltonian as

$$H'_{\text{el-ph}} = 2\lambda n_{\text{ap}} \sqrt{n_\beta(C)} (u_C + v_C) (B_C + B_C^\dagger),$$

where we used the numerical result from Fig. 2(b) that  $n_{\text{el}}(L) = n_{\text{el}}(R)$  for all  $K$  to simplify the notation to  $n_{\text{ap}}$ , the electronic occupation in the apical positions of the cluster. Finally, in terms of the Bogoliubov coefficients and together with diagonal part (B11), the newly transformed Hamiltonian with a novel central electron-phonon coupling is written as  $H' = H'_d + H'_{\text{el-ph}}$ ,

$$H' = \hbar F(K) B_C^\dagger B_C + \lambda' n_{\text{ap}} (B_C + B_C^\dagger),$$

where the new coupling depends on the central Sr-phonon related occupation  $n_\beta(C)$  as

$$\lambda' = \frac{2\lambda \sqrt{n_\beta(C)}}{\sqrt{2A\gamma}} (\sqrt{\omega + \gamma} + \sqrt{\omega - \gamma}). \quad (\text{B11})$$

To summarize, by separating the  $\text{O}_{\text{ap}}\text{-Sr-O}_{\text{ap}}$  triatomic molecule and using a nonlinear, multimodal Bogoliubov transformation, we started with two oscillator communities associated with  $b_L, b_L^\dagger$  and  $b_R, b_R^\dagger$  phonon modes, but we ended up with three oscillator communities, with the addition of the modes associated with  $B_C, B_C^\dagger$ . This introduces a novel central phonon, located in the plane and related to the planar oxygen oscillations, together with the original left and right oscillations of the apical oxygens. Furthermore, those novel planar vibrational modes couple to the electronic degrees of freedom with a renormalized electron-phonon coupling given by Eq. (B11), which gives rise to a new IQTP mode, now located in the copper oxide plane. To see how exactly the new phonon,  $B_C$ , couples to the central oxygen atom,  $\text{O}_{\text{pl}}$ , let us recall that within our 6-atom cluster one has a single excess hole for all oxygen atoms

$$2n_{\text{ap}} + n_C = 1 \rightarrow n_{\text{ap}} = \frac{1 - n_C}{2}, \quad (\text{B12})$$

where  $n_C$  is the electronic occupation of the planar  $\text{O}_{\text{pl}}$  at the center of the cluster. So, after applying the nonlinear Bogoliubov transformation we rewrite the central contribution of the electron-phonon transformed Hamiltonian in a way that the new phonon  $B_C$  couples to the central oxygen atom, via its occupation, after the synchronization transition, when  $n_\beta(C) > 0$ . Therefore, after a multimodal, nonlinear Bogoliubov transformation, not only a newly phonon mode, associated with the planar oxygen displacements, appears, but it also couples to the excess charge pumped to the central site, giving rise to an extension of the IQTPs to the plane and allowing the description of the problem to be summarized in the triple-well potential interpretation.

[1] H. S. Obhi and E. K. H. Salje, Effect of the metal-superconductor phase transition and Co doping on the phonon spectra of  $\text{YBa}_2\text{Cu}_3\text{O}_{7-\delta}$ , *Physica C* **171**, 547 (1990).

[2] B. K. Guttler, E. K. H. Salje, P. Freeman, J. Blunt, M. Harris, T. Duffield, C. D. Ager, and H. P. Hughes, Critical behavior of bulk phonons in  $\text{YBa}_2\text{Cu}_3\text{O}_{7-\delta}$  as observed by infrared

- absorption spectroscopy, *J. Phys.: Condens. Matter* **2**, 8977 (1990).
- [3] N. N. Kovaleva, A. V. Boris, T. Holden, C. Ulrich, B. Liang, C. T. Lin, B. Keimer, C. Bernhard, J. L. Tallon, D. Munzar, and A. M. Stoneham, *c*-axis lattice dynamics in Bi-based cuprate superconductors, *Phys. Rev. B* **69**, 054511 (2004).
- [4] S. Sugai, H. Suzuki, Y. Takayanagi, T. Hosokawa, and N. Hayamizu, Carrier-density-dependent momentum shift of the coherent peak and the LO phonon mode in *p*-type high- $T_c$  superconductors, *Phys. Rev. B* **68**, 184504 (2003).
- [5] D. Reznik, L. Pintschovius, M. Ito, S. Iikubo, M. Sato, H. Goka, M. Fujita, K. Yamada, G. D. Gu, and J. M. Tranquada, Electron-phonon coupling reflecting dynamic charge inhomogeneity in copper oxide superconductors, *Nature (London)* **440**, 1170 (2006).
- [6] T. Cuk, D. H. Lu, X. J. Zhou, Z.-X. Shen, T. P. Devereaux, and N. Nagaosa, A review of electron-phonon coupling seen in the high- $T_c$  superconductors by angle-resolved photoemission studies (ARPES), *Phys. Status Solidi (b)* **242**, 11 (2005).
- [7] W. Meevasana, N. J. C. Ingle, D. H. Lu, J. R. Shi, F. Baumberger, K. M. Shen, W. S. Lee, T. Cuk, H. Eisaki, T. P. Devereaux, N. Nagaosa, J. Zaanen, and Z.-X. Shen, Doping Dependence of the Coupling of Electrons to Bosonic Modes in the Single-Layer High-Temperature  $\text{Bi}_2\text{Sr}_2\text{CuO}_6$  Superconductor, *Phys. Rev. Lett.* **96**, 157003 (2006).
- [8] Y. He, M. Hashimoto, D. Song, S.-D. Chen, J. He, I. M. Vishik, B. Moritz, D.-H. Lee, N. Nagaosa, J. Zaanen, T. P. Devereaux, Y. Yoshida, H. Eisaki, D. H. Lu, and Z.-X. Shen, Rapid change of superconductivity and electron-phonon coupling through critical doping in Bi-2212, *Science* **362**, 62 (2018).
- [9] A. Lanzara, P. V. Bogdanov, X. J. Zhou, S. A. Kellar, D. L. Feng, E. D. Lu, T. Yoshida, H. Eisaki, A. Fujimori, K. Kishio, J.-I. Shimoyama, T. Noda, S. Uchida, Z. Hussain, and Z.-X. Shen, Evidence for ubiquitous strong electron-phonon coupling in high-temperature superconductors, *Nature (London)* **412**, 510 (2001).
- [10] M. Le Tacon, A. Bosak, S. M. Souliou, G. Dellea, T. Loew, R. Heid, K.-P. Bohnen, G. Ghiringhelli, M. Krisch, and B. Keimer, Inelastic x-ray scattering in  $\text{YBa}_2\text{Cu}_3\text{O}_{6.6}$  reveals giant phonon anomalies and elastic central peak due to charge-density-wave formation, *Nat. Phys.* **10**, 52 (2014).
- [11] L. Chaix, G. Ghiringhelli, Y. Y. Peng, M. Hashimoto, B. Moritz, K. Kummer, N. B. Brookes, Y. He, S. Chen, S. Ishida, Y. Yoshida, H. Eisaki, M. Salluzzo, L. Braicovich, Z.-X. Shen, T. P. Devereaux, and W.-S. Lee, Dispersive charge density wave excitations in  $\text{Bi}_2\text{Sr}_2\text{CaCu}_2\text{O}_{8+\delta}$ , *Nat. Phys.* **13**, 952 (2017).
- [12] Y. He, S. Wu, Y. Song, W.S. Lee, A. H. Said, A. Alatas, A. Bosak, A. Girard, S. M. Souliou, A. Ruiz, M. Hepting, M. Bluschke, E. Schierle, E. Weschke, J. S. Lee, H. Jang, H. Huang, M. Hashimoto, D. H. Lu, D. Song, Y. Yoshida, H. Eisaki, Z.X. Shen, R. J. Birgeneau, M. Yi, and A. Frano, Persistent low-energy phonon broadening near the charge-order  $q$  vector in the bilayer cuprate  $\text{Bi}_2\text{Sr}_2\text{CaCu}_2\text{O}_{8+\delta}$ , *Phys. Rev. B* **98**, 035102 (2018).
- [13] T. Egami, Real-space description of dynamics of liquids, *Quantum Beam Sci.* **2**, 22 (2018).
- [14] T. Egami, B. H. Toby, S. J. L. Billinge, H. D. Rosenfeld, J. D. Jorgensen, D. G. Hinks, B. Dabrowski, M. A. Subramanian, M. K. Crawford, W. E. Farneth, and E. M. McCarron, Local structural anomaly near  $T_c$  observed by pulsed neutron scattering, *Physica C* **185-189**, 867 (1991).
- [15] M. Arai, K. Yamada, S. Hosoya, A. C. Hannon, Y. Hidaka, A. D. Taylor, and Y. Endoh, Local structural instability of high- $T_c$  oxide superconductors studied by inelastic neutron scattering, *J. Supercond.* **7**, 415 (1994).
- [16] M. I. Salkola, A. R. Bishop, S. A. Trugman, and J. M. Deleon, Correlation-function analysis of nonlinear and nonadiabatic systems: Polaron tunneling, *Phys. Rev. B* **51**, 8878 (1995).
- [17] J. M. de Leon, S. D. Conradson, T. Tyson, A. R. Bishop, M. Salkola, F. J. Espinosa, and J. L. Pena, X-ray absorption fine structure applied to the study of systems with lattice instabilities, *MRS Online Proc. Libr.* **437**, 189 (1996).
- [18] S. D. Conradson, I. D. Raistrick, and A. R. Bishop, Axial oxygen centered lattice instabilities and high-temperature superconductivity, *Science* **248**, 1394 (1990).
- [19] J. M. de Leon, S. D. Conradson, I. Batistic, and A. R. Bishop, Evidence for an Axial Oxygen-Centered Lattice Fluctuation Associated with the Superconducting Transition in  $\text{YBa}_2\text{Cu}_3\text{O}_7$ , *Phys. Rev. Lett.* **65**, 1675 (1990).
- [20] P. G. Allen, J. M. de Leon, S. D. Conradson, and A. R. Bishop, Characterization of a split axial-oxygen site in  $\text{TlBa}_2\text{Ca}_3\text{Cu}_4\text{O}_{11}$  by extended x-ray-absorption fine-structure spectroscopy, *Phys. Rev. B* **44**, 9480 (1991).
- [21] J. M. de Leon, S. D. Conradson, I. Batistic, and A. R. Bishop, Correlation between axial-oxygen anharmonicity and  $T_c$  in  $\text{YBa}_2\text{Cu}_3\text{O}_7$  and related compounds, *Phys. Rev. B* **44**, 2422 (1991).
- [22] J. M. de Leon, I. Batistic, A. R. Bishop, S. D. Conradson, and S. A. Trugman, Polaron Origin for Anharmonicity of the Axial Oxygen in  $\text{YBa}_2\text{Cu}_3\text{O}_7$ , *Phys. Rev. Lett.* **68**, 3236 (1992).
- [23] J. M. de Leon, S. D. Conradson, I. Batistic, A. R. Bishop, I. D. Raistrick, M. C. Aronson, and F. H. Garzon, Axial oxygen-centered lattice instabilities in  $\text{YBa}_2\text{Cu}_3\text{O}_7$ : An application of the analysis of extended x-ray-absorption fine-structure in anharmonic systems, *Phys. Rev. B* **45**, 2447 (1992).
- [24] C. H. Booth, F. Bridges, J. B. Boyce, T. Claeson, B. M. Lairson, R. Liang, and D. A. Bonn, Comparison of local structure measurements from *c*-axis polarized XAFS between a film and a single crystal of  $\text{YBa}_2\text{Cu}_3\text{O}_{7-\delta}$  as a function of temperature, *Phys. Rev. B* **54**, 9542 (1996).
- [25] J. M. de Leon, G. G. Li, S. Conradson, A. Bishop, M. Subramanian and I. Raistrick, Planar oxygen-centered lattice instabilities in TI-based high-temperature superconductors, *Physica C* **220**, 377 (1994).
- [26] A. Bianconi, M. Missori, H. Oyanagi, H. Yamaguchi, D. H. Ha, Y. Nishihara, and S. Della Longa, The measurement of the polaron size in the metallic phase of cuprate superconductors, *Europhys. Lett.* **31**, 411 (1995).
- [27] A. Bianconi, N. L. Saini, A. Lanzara, M. Missori, T. Rossetti, H. Oyanagi, H. Yamaguchi, K. Oka, and T. Ito, Determination of the Local Lattice Distortions in the  $\text{CuO}_2$  Plane of  $\text{La}_{1.85}\text{Sr}_{0.15}\text{CuO}_4$ , *Phys. Rev. Lett.* **76**, 3412 (1996).
- [28] A. Bianconi, N. L. Saini, T. Rossetti, A. Lanzara, A. Perali, M. Missori, H. Oyanagi, H. Yamaguchi, Y. Nishihara, and D. H. Ha, Stripe structure in the  $\text{CuO}_2$  plane of perovskite superconductors, *Phys. Rev. B* **54**, 12018 (1996).
- [29] S. D. Conradson, J. M. De Leon and A. R. Bishop, Local phase separation in TI-based oxide superconductors, *J. Supercond.* **10**, 329 (1997).

- [30] M. Acosta-Alejandra, J. M. de Leon, S. D. Conradson and A. R. Bishop, Evidence for a local structural change in  $\text{La}_2\text{CuO}_{4.1}$  across the superconducting transition, *J. Supercond.* **15**, 355 (2002).
- [31] J. M. de Leon, M. Acosta-Alejandra, S. D. Conradson and A. R. Bishop, Change of the in-plane Cu-O bond distribution in  $\text{La}_2\text{CuO}_{4.1}$  across  $T_c$ , *J. Phys. Chem. Solids* **69**, 2288 (2008).
- [32] H. Oyanagi, C. Zhang, A. Tsukada, and M. Naito, Lattice instability in high-temperature superconducting cuprates: Polarons probed by EXAFS, *J. Supercond. Novel Magn.* **22**, 165 (2009).
- [33] A. P. Menushenkov, K. V. Klementev, P. V. Konarev, A. A. Meshkov, S. Benazeth, and J. Purans, The double-well oscillating potential of oxygen atoms in perovskite system  $\text{Ba}(\text{K})\text{BiO}_3$ : EXAFS-analysis results, *Nucl. Instrum. Methods Phys. Res., Sect. A* **448**, 340 (2000).
- [34] A. P. Menushenkov and K. V. Klementev, Extended x-ray absorption fine-structure indication of a double-well potential for oxygen vibration in  $\text{Ba}_{1-x}\text{K}_x\text{BiO}_3$ , *J. Phys.: Condens. Matter* **12**, 3767 (2000).
- [35] V. G. Ivanov, A. A. Ivanov, A. P. Menushenkov, B. Joseph, and A. Bianconi, Fe-As bond fluctuations in a double-well potential in  $\text{LaFeAsO}$ , *J. Supercond. Novel Magn.* **29**, 3035 (2016).
- [36] C. J. Zhang and H. Oyanagi, Local lattice instability and superconductivity in  $\text{La}_{1.85}\text{Sr}_{0.15}\text{Cu}_{1-x}\text{M}_x\text{O}_4$  ( $M = \text{Mn}, \text{Ni}, \text{and Co}$ ), *Phys. Rev. B* **79**, 064521 (2009).
- [37] S. D. Conradson, Theodore H. Geballe, Changqing Jin, Lipeng Cao, Gianguido Baldinozzi, Jack M. Jiang, Matthew J. Latimer, and Oliver Mueller, Local structure of  $\text{Sr}_2\text{CuO}_{3.3}$ , a 95 K cuprate superconductor without  $\text{CuO}_2$  planes, *Proc. Natl. Acad. Sci. USA* **117**, 4565 (2020).
- [38] A. R. Bishop, D. Mihailovic, and J. M. de Leon, Signatures of mesoscopic Jahn-Teller polaron inhomogeneities in high-temperature superconductors, *J. Phys.: Condens. Matter* **15**, L169 (2003).
- [39] E. W. Huang, C. B. Mendl, S. Liu, S. Johnston, H.-C. Jiang, B. Moritz, and T. P. Devereaux, Numerical evidence of fluctuating stripes in the normal state of high- $T_c$  cuprate superconductors, *Science* **358**, 1161 (2017).
- [40] S. Kim, X. Chen, W. Fitzhugh and X. Li, Apical Charge Flux-Modulated In-Plane Transport Properties of Cuprate Superconductors, *Phys. Rev. Lett.* **121**, 157001 (2018).
- [41] D. Haskel, E. A. Stern, D. G. Hinks, A. W. Mitchell, and J. D. Jorgensen, Altered Sr environment in  $\text{La}_{2-x}\text{Sr}_x\text{CuO}_4$ , *Phys. Rev. B* **56**, R521(R) (1997).
- [42] S. D. Conradson, V. Velasco, M. B. Silva Neto, T. H. Geballe, C.-Q. Jin, W.-M. Li, L.-P. Cao, A. Gauzzi, M. Karppinen, A. Perali, S. Wimberger, A. R. Bishop, G. Baldinozzi, M. Latimer, and E. Gilioli, Correlation of strontium anharmonicity with charge-lattice dynamics of the apical oxygens and their coupling to cuprate superconductivity, [arXiv:2109.14092](https://arxiv.org/abs/2109.14092).
- [43] J. A. Acebron, L. L. Bonilla, C. J. Pérez Vicente, F. Ritort, and R. Spigler, The Kuramoto model: A simple paradigm for synchronization phenomena, *Rev. Mod. Phys.* **77**, 137 (2005).
- [44] M. Capone, W. Stephan, and M. Grilli, Small-polaron formation and optical absorption in Su-Schrieffer-Heeger and Holstein models, *Phys. Rev. B* **56**, 4484 (1997).
- [45] V. Velasco, M. B. Silva Neto, A. Perali, S. Wimberger, A. R. Bishop, and S. D. Conradson, Evolution of charge-lattice dynamics across the Kuramoto synchronization phase diagram of quantum tunneling polarons in cuprate superconductors, *Condens. Matter* **6**, 52 (2021).
- [46] S. D. Conradson, T. H. Geballe, A. Gauzzi, M. Karppinen, C. Jin, G. Baldinozzi, W. Li, L. Cao, E. Gilioli, J. M. Jiang, M. Latimer, O. Mueller, and V. Nasretdinova, Local lattice distortions and dynamics in extremely overdoped superconducting  $\text{YSr}_2\text{Cu}_{2.75}\text{Mo}_{0.25}\text{O}_{7.54}$ , *Proc. Natl. Acad. Sci. USA* **117**, 4559 (2020).
- [47] Y. Kuramoto, Self-entrainment of a population of coupled nonlinear oscillators, *Lect. Notes Phys.* **39**, 420 (1975).
- [48] J. Pantaleone, Synchronization of metronomes, *Am. J. Phys.* **70**, 992 (2002).
- [49] P. Tass, A model of desynchronizing deep brain stimulation with a demand-controlled coordinated reset of neural subpopulations, *Biol. Cybern.* **89**, 81 (2003).
- [50] G. Jongen, J. Anemüller, D. Bollé, A. C. C. Coolen, and C. Pérez-Vicente, Coupled dynamics of fast spins and slow exchange interactions in the  $XY$  spin glass, *J. Phys. A: Math. Gen.* **34**, 3957 (2001).
- [51] K. Wiesenfeld, P. Colet, and S. H. Strogatz, Frequency locking in Josephson arrays: Connection with the Kuramoto model, *Phys. Rev. E* **57**, 1563 (1998).
- [52] D. Witthaut, S. Wimberger, R. Burioni, and M. Timme, Classical synchronization indicates persistent entanglement in isolated quantum systems, *Nat. Commun.* **8**, 14829 (2017).
- [53] V. Velasco and M. B. Silva Neto, Unconventional superconductivity as a quantum Kuramoto synchronization problem in random elasto-nuclear oscillator networks, *J. Phys. Commun.* **5**, 015003 (2021).
- [54] G. Paleari, F. Hébert, B. Cohen-Stead, K. Barros, R. T. Scalettar, and G. G. Batrouni, Quantum Monte Carlo study of an anharmonic Holstein model, *Phys. Rev. B* **103**, 195117 (2021).
- [55] A. Chatterjee and Y. Takada, The Hubbard-Holstein Model with Anharmonic Phonons in One Dimension, *J. Phys. Soc. Jpn.* **73**, 964 (2004).
- [56] Ch. U. Lavanya, I. V. Sankar, and A. Chatterjee, Metallicity in a Holstein-Hubbard chain at half filling with Gaussian anharmonicity, *Sci. Rep.* **7**, 3774 (2017).
- [57] D. Emin, *Polarons* (Cambridge University Press, Cambridge, 2012).
- [58] W. M. Li, J. F. Zhao, L. P. Cao, Z. Hu, Q. Z. Huang, X. C. Wang, Y. Liu, G. Q. Zhao, J. Zhang, Q. Q. Liu *et al.*, Superconductivity in a unique type of copper oxide, *Proc. Natl. Acad. Sci. USA* **116**, 12156 (2019).
- [59] S. D. Conradson, T. H. Geballe, C.-Q. Jin, L.-P. Cao, A. Gauzzi, M. Karppinen, G. Baldinozzi, W.-M. Li, E. Gilioli, J. M. Jiang, M. Latimer, O. Mueller, and V. Nasretdinova, Nonadiabatic coupling of the dynamical structure to the superconductivity in  $\text{YSr}_2\text{Cu}_{2.75}\text{Mo}_{0.25}\text{O}_{7.54}$  and  $\text{Sr}_2\text{CuO}_{3.3}$ , *Proc. Natl. Acad. Sci. USA* **117**, 33099 (2020).